

Development of a low-cost multifunctional wireless impedance sensor node

Jiyoung Min¹, Seunghee Park², Chung-Bang Yun^{1*} and Byunghun Song³

¹Department of Civil and Environmental Engineering, KAIST, South Korea

²Department of Civil and Environmental Engineering, Sungkyunkwan University, South Korea

³RFID-USN Convergence Research Center, Korea Electronics Technology Institute, South Korea

(Received November 12, 2009, Accepted February 20, 2010)

Abstract. In this paper, a low cost, low power but multifunctional wireless sensor node is presented for the impedance-based SHM using piezoelectric sensors. Firstly, a miniaturized impedance measuring chip device is utilized for low cost and low power structural excitation/sensing. Then, structural damage detection/sensor self-diagnosis algorithms are embedded on the on-board microcontroller. This sensor node uses the power harvested from the solar energy to measure and analyze the impedance data. Simultaneously it monitors temperature on the structure near the piezoelectric sensor and battery power consumption. The wireless sensor node is based on the TinyOS platform for operation, and users can take MATLAB[®] interface for the control of the sensor node through serial communication. In order to validate the performance of this multifunctional wireless impedance sensor node, a series of experimental studies have been carried out for detecting loose bolts and crack damages on lab-scale steel structural members as well as on real steel bridge and building structures. It has been found that the proposed sensor nodes can be effectively used for local wireless health monitoring of structural components and for constructing a low-cost and multifunctional SHM system as “place and forget” wireless sensors.

Keywords: structural health monitoring; piezoelectric sensor; electromechanical impedance; wireless sensor node; multifunctional system.

1. Introduction

On-line structural health monitoring (SHM) has become an important issue in civil, mechanical and aerospace engineering fields. Particularly, the interest in health monitoring for critical members of large structures is dramatically growing with increasing social needs. To date, numerous techniques and algorithms have been proposed for local SHM with smart sensors including fiber optic sensors and piezoelectric sensors. Among them, the electromechanical (E/M) impedance-based SHM has shown promising results for steel structures (Park *et al.* 2003, Park *et al.* 2005, Koo *et al.* 2009, Park *et al.* 2009a, Taylor *et al.* 2009a, b). The technique utilizes small piezoelectric sensors such as piezoceramic (PZT) and macro-fiber composite (MFC) patches attached to a structure as self-sensing actuators to both excite the structure with high-frequency sweeping and monitor any changes in structural mechanical impedance (Giurgiutiu *et al.* 1999, Park *et al.* 2003, Park *et al.* 2009a). By monitoring the

*Corresponding Author, Professor, E-mail: ycb@kaist.ac.kr

electrical impedance of the PZT, assessments can be made about the integrity of the structure. Recent advances in online SHM, including actuation and sensing, on-board computing, and radio-frequency (RF) telemetry, have improved the accessibility of the impedance method for in-field measurements. Lynch *et al.* (2004) designed a wireless active sensing unit to monitor civil structures, which was constructed of off-the-shelf components and had the ability to command active sensors and actuators from a computational core combined with wireless transmission and sensing circuits, embedded algorithm to process the acquired data, and structural status broadcasting. Grisso and Inman (2005) designed a DSP (Digital Signal Processor) based prototype to provide wireless assessment of thermal protection systems. It was able to directly detect damages by analyzing variations of the electrical impedance of PZT sensors bonded to the structure. The obtained impedance signals were compared with the pre-stored baseline and a statistical damage index was calculated. Mascarenas *et al.* (2007) proposed a wireless sensor node which consists of a miniaturized impedance measuring chip, a microprocessor, and a radio-frequency identification (RFID) module. Low cost impedance measuring chip actuated the structure through a PZT and measured the structural impedance response, and RFID module delivered the diagnostic result to a base station. Park *et al.* (2009a) improved the wireless sensor node of Mascarenas *et al.* (2007) by adding two multiplexer IC chips for 16 channels for the cases of multiple sensors in a small region and by embedding signal processing algorithms in the microcontroller unit (MCU) for both structural damage identification and sensor self-diagnosis. Research groups at Los Alamos National Lab recently developed a compact impedance-based wireless sensing device (WID3) for low power operation (Overly *et al.* 2007, 2008), which requires around 60 mW of power to operate. Here, a wake-up capability was combined for low power operation. Taylor *et al.* (2009a, b) extended the capability of the WID3 by implementing a module with low-frequency A/D and D/A converters to measure low-frequency vibration data for multiple SHM techniques. It is wirelessly triggered by a mobile agent for use in the mobile-host-based wireless sensing network. The mobile agent also provides computational power to real-time assessments on the structural conditions.

Based on these prior researches, this paper extends the impedance-based wireless SHM node for the purpose of multifunctional and environment-friendly uses in SHM applications. More specifically this study focuses on the following three objectives: (1) to develop in-field adjustable impedance-based wireless sensor nodes with on-board algorithms for structural and sensor-self diagnosis, (2) to incorporate the energy scavenging system for maintenance-free wireless sensor node, and (3) to investigate the feasibility of the impedance-based SHM system to real structures. A series of experimental studies are performed to determine the capability of the sensor node to monitor the health of sensors and structures. First, lab tests are carried out to validate the acquired data from the developed wireless sensor nodes. Tests are done for detecting a growing crack on a steel truss member, and for monitoring the sensor fracture and the bonding layer damage for sensor self-diagnosis. Finally, the wireless system is utilized in an attempt to detect loose bolts and crack damages occurrence in real buildings and bridge structures.

2. Theoretical backgrounds

2.1 Electromechanical impedance-based SHM techniques

The E/M impedance-based SHM techniques have been developed as a promising tool for real-time structural damage assessment on critical members of large structural systems (Park *et al.* 2003, Koo *et*

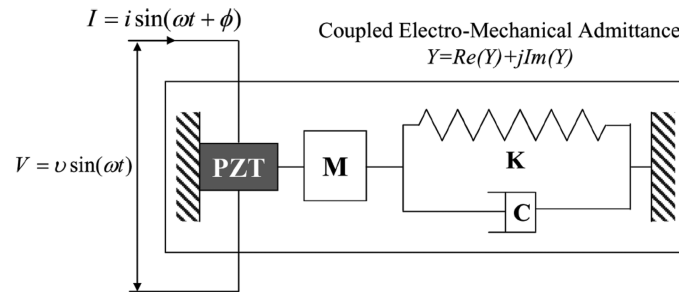


Fig. 1 1-D Model used to derive electromechanical admittance of a PZT bonded to a structure (Liang *et al.* 1996)

al. 2009, Taylor *et al.* 2009a, b, Mascarenas *et al.* 2009). They make use of piezoelectric sensors such as piezoceramic (PZT) and macro-fiber composite (MFC) patches, which form a collocated sensor and actuator, often referred to as a self-sensing actuator (Giurgiutiu 2008). The basis of this active sensing technology is the energy transfer between the actuator and the host mechanical system. If a PZT attached on a structure is driven with a sinusoidal voltage, it causes the local area of the structure to vibrate (the converse piezoelectric effect). And the structural response causes an electrical response in the PZT (the direct piezoelectric effect). Liang *et al.* (1994) first proposed a one-dimensional analytical model of this setup as in Fig. 1, and showed that the electrical admittance (inverse of the electrical impedance), $Y(\omega)$, of a PZT is directly correlated to the local mechanical impedance of the host structure, $Z_s(\omega)$, and that of a PZT patch, $Z_a(\omega)$, in most applications as

$$Y(\omega) = G(\omega) + jB(\omega) = j\omega C \left(1 - \kappa_{31}^2 \frac{Z_s(\omega)}{Z_s(\omega) + Z_a(\omega)} \right) \quad (1)$$

where G is the conductance (real part); B is the susceptance (imaginary part); C is the zero-load capacitance of a PZT; and κ_{31} is the electromechanical coupling coefficient of a PZT. Given that the mechanical impedance and the material properties of the PZT stay constant, the equation shows that a change in the structure's mechanical impedance directly results in a change in the electrical impedance measured by the PZT. Since damages cause a change in the structure's local mass, stiffness, or damping properties and consequently its mechanical impedance, the structure's mechanical integrity can be assessed by monitoring the PZT's electrical impedance. It should be noted that the admittance function, $Y(\omega)$, is a complex number. Bhalla *et al.* (2002) demonstrated that the real part of the measured admittance is more sensitively changed due to the structural damage condition as compared to the imaginary part. On the other hand, Park *et al.* (2006) found out that the imaginary part can be more effectively used for piezoelectric sensor self-diagnosis.

2.2 Statistical damage indices for damage detection: RMSD and cross-correlation coefficient

By observing some changes of the E/M impedance acquired from a PZT attached on a host structure, assessments can be made about the integrity of the host structure. Since the impedance changes provide only a qualitative assessment for damage detection, several scalar damage metrics have been used for quantitative measure of structural damages. Peairs *et al.* (2006) compares several damage metrics, while the most commonly used indices for the impedance method are the root mean square deviation (RMSD) and the cross-correlation coefficient (CC) as

$$RMSD = \sqrt{\frac{\sum_{i=1}^n \{ \text{Re}(Z_0(\omega_i) - \bar{Z}_0) - (\text{Re}(Z_1(\omega_i)) - \bar{Z}_1) \}^2}{\sum_{i=1}^n \text{Re}(Z_0(\omega_i) - \bar{Z}_0)^2}} \quad (2)$$

$$CC = \frac{1}{N} \sum_{i=1}^N \frac{\{ \text{Re}(Z_0(\omega_i)) - \bar{Z}_0 \} \{ \text{Re}(Z_1(\omega_i)) - \bar{Z}_1 \}}{\sigma_{Z_0} \sigma_{Z_1}} \quad (3)$$

where $Z_0(\omega)$ is the impedance of the PZT measured in the healthy condition (baseline); $Z_1(\omega)$ is the impedance in the concurrent condition; n is the number of frequency points; \bar{Z}_0 and \bar{Z}_1 are the mean values of the real parts of $Z_0(\omega)$ and $Z_1(\omega)$; and σ_{Z_0} and σ_{Z_1} are the standard deviations of the real parts of $Z_0(\omega)$ and $Z_1(\omega)$. These metrics are scaled by the baseline measurement, $Z_0(\omega)$, and are corrected for the vertical shift between measurements by subtracting mean values. The vertical shift is mainly caused by changes in environmental conditions such as temperature and humidity (Koo *et al.* 2009). Greater numerical value of the RMSD metric indicates larger difference between the baseline reading and the subsequent reading, which indicates clearer presence of damage in the structure. On the other hand, smaller value of the CC metric indicates larger difference between the impedances and clearer presence of damage.

Temperature variation due to surrounding changes should be considered with careful attention because it may result in a significant impedance variation, particularly a frequency shift in the impedance, which may lead to erroneous diagnostic results of real structures. To date, several studies have been reported to avoid the temperature variation effects on the impedance measurement. Bhalla *et al.* (2002) investigated the influence of the structure-actuator interactions and temperature variation on the impedance signatures. Koo *et al.* (2009) proposed the effective frequency shift (EFS; $\tilde{\omega}$) method in order to compensate temperature effects on impedances, which is based on the frequency shift giving the maximum cross-correlation coefficient between the baseline impedance data, $Z_0(\omega)$, and the concurrent impedance data, $Z_1(\omega)$, as

$$CC = \max_{\tilde{\omega}} \left\{ \frac{1}{N} \sum_{i=1}^N \frac{\{ \text{Re}(Z_0(\omega_i)) - \bar{Z}_0 \} \{ \text{Re}(Z_1(\omega_i - \tilde{\omega})) - \bar{Z}_1 \}}{\sigma_{Z_0} \sigma_{Z_1}} \right\} \quad (4)$$

Fig. 2(a) shows that the temperature change causes considerable variation with both vertical and horizontal shifts on two impedance measurements at the same damage condition. As the EFS method is applied to compensate the temperature effect, excellent match can be obtained between two signatures as shown in Fig. 2(b). Here, the effect of the vertical shift in the measured signal is automatically compensated by subtracting the mean values as in Eqs. (3) and (4).

2.3 Piezoelectric sensor self-diagnosis

PZT sensors attached to a structure play a major role in the successful operation of a health monitoring and damage-detection system. The integrity of the sensor and the consistency of the sensor/structure interface are essential elements that can ‘make or break’ structural monitoring (Giurgiutiu 2008). For real structures, the duration of the monitoring process is extensive and

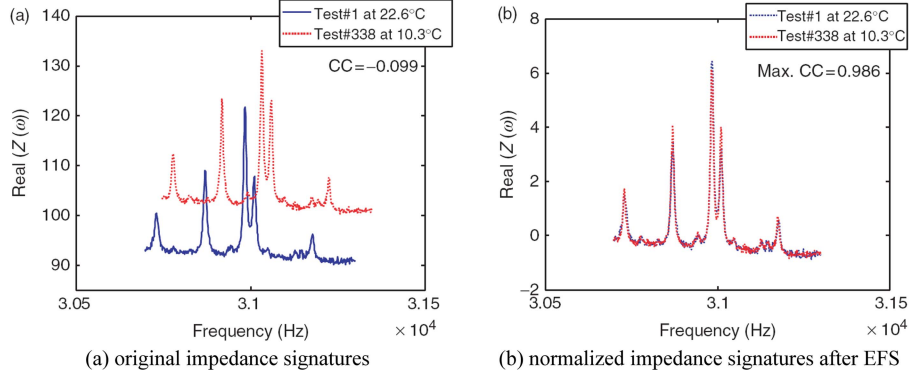


Fig. 2 Temperature compensation using EFS method (Koo *et al.* 2009)

can span several years. It also encompasses various service conditions and several loading cases. Therefore, the sensor self-diagnostic procedure, where sensors/actuators are confirmed to be operational, is critically important for the successful implementation of the SHM system. Since most of the PZT patches are brittle, sensor fracture and subsequent degradation of mechanical/electrical properties are common types of the PZT sensor failures. In addition, the integrity of the bonding layer between a PZT and a host structure should be maintained and monitored throughout their service lives.

Saint-Pierre *et al.* (1996) and Giurgiutiu *et al.* (2002) proposed a de-bonding identification algorithm by monitoring the resonance of a PZT sensor measured by electrical impedances. As the de-bonding area between the PZT and the host increases, the shape of the PZT's resonance becomes sharper and more distinctive, and the magnitudes of the host resonances get reduced. Park *et al.* (2006) introduced a piezoelectric sensor-diagnostic procedure based on tracking the imaginary part of the measured electrical admittance, which can be justified by the fact that the PZT is a capacitive device and its admittance is dominated by the imaginary part ($j\omega C$) in Eq. (1). This study demonstrated that bonding defects affect the measured admittance and can be identified by monitoring the slope of the admittance. Bonding defects would cause an upward shift in the slope of the imaginary part of the admittance, while sensor breakage would cause a downward shift in the slope implying the decrease of the capacitive value of the PZT. Therefore, sensor functionality including the sensor breakage and the degradation of the bonding condition could be assessed by monitoring the imaginary part of the admittance. Park *et al.* (2009b) proposed a modified impedance model adding three parameters to Eq. (1) for PZT sensor self-diagnosis, which considers the effect of the bonding layer between a PZT and a host on the dynamic interaction in the coupled electromechanical system as

$$\tilde{Y}(\omega) = j\omega a C \left(1 - b k_{31}^2 \frac{\xi \cdot Z_s(\omega)}{\xi \cdot Z_s(\omega) + Z_a(\omega)} \right) \quad (5)$$

where a is the sensor quality index ($0 \leq a \leq 1$); b is the bonding degradation index ($0 \leq b \leq 1$); $\xi = 1/(1 + K_s/K_b)$ is the shear-lag index between a bonding layer and a host structure ($0 \leq \xi \leq 1$); and K_s and K_b are dynamic stiffnesses of the host structure and the bonding layer, respectively.

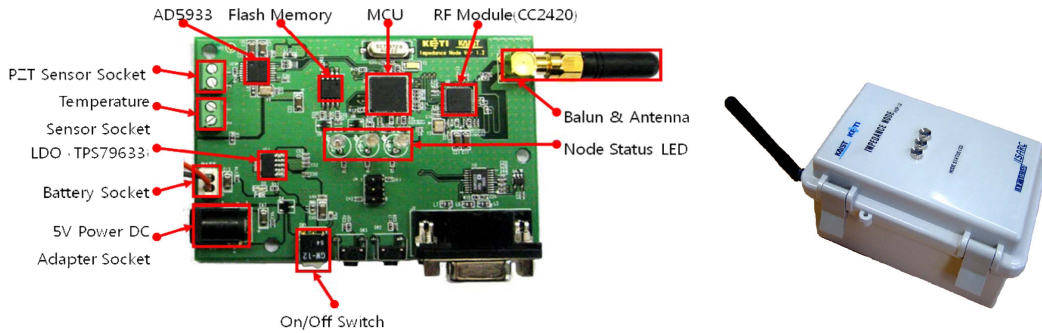
3. Development of wireless impedance sensor nodes

3.1 Subsystems of wireless impedance sensor nodes

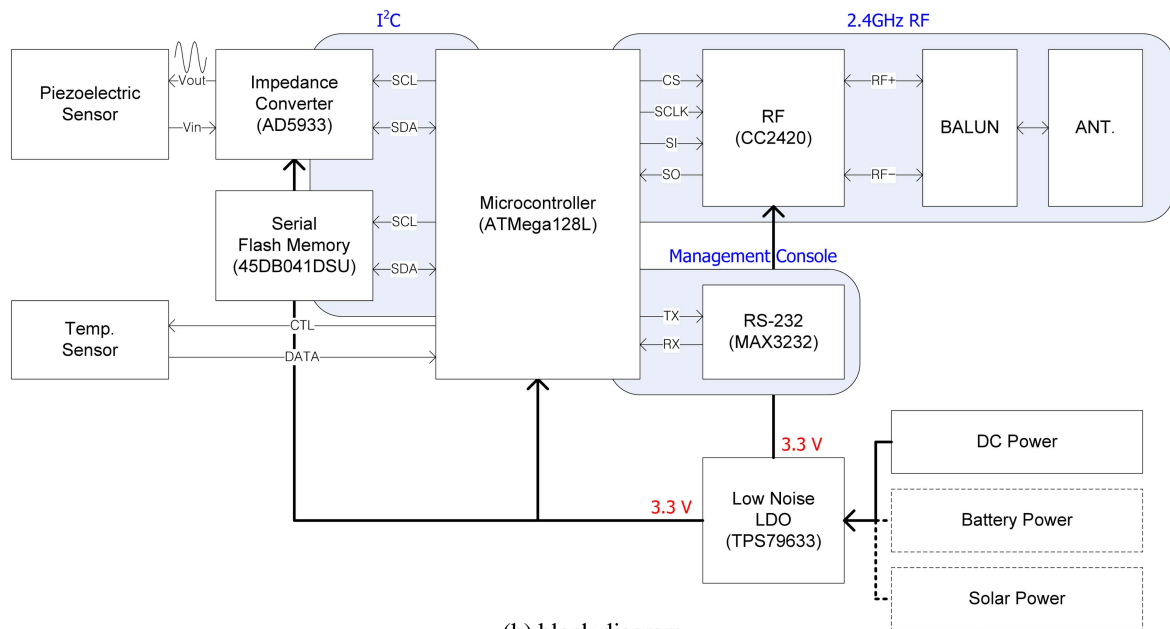
To measure the E/M impedances, impedance analyzers such as HP4194A/HP4294A are conventionally used. However, they are not quite suitable for field applications to online SHM because they are bulky (approximately 25 kg) and expensive (approximately 40,000 USD). Thus, research on the impedance-based SHM technique trends toward development of self-contained sensors and wireless active sensor nodes with all required functions including actuating/sensing, data processing, damage assessments and sensor self-diagnostics on the sensor board as well as power management with energy harvesters. Recently, Analog Devices[®] developed an integrated impedance converters, AD5933 (www.analog.com). It is equipped with a 12-bit analog-to-digital converter (ADC), a digital-to-analog converter (DAC) and a discrete Fourier transform (DFT) functionality. The frequency generator allows an external complex impedance with range of 100 Ω to 10 M Ω to be excited with a known frequency of up to 100 kHz. AD5933 is just of a penny size, thus it provides a solution for self-contained miniaturized impedance measuring. Therefore, AD5933 has been used as a core component in developing a wireless impedance sensor node for SHM applications (Mascarenas *et al.* 2007, 2009, Overly *et al.* 2007, 2008, Taylor *et al.* 2009a, b, Park *et al.* 2009a).

The wireless sensor node, proposed in this paper, has extended the previous researches for multifunctional and environment-friendly uses in the impedance-based SHM (Mascarenas *et al.* 2007, Park *et al.* 2009a). It was designed by adding: (1) optimal arrangement of each chip for low power consumption, (2) energy harvester equipped with solar panels, (3) peer-to-peer communication by using a RF transceiver of CC2420, which enables to construct the ubiquitous sensor network, (4) internal algorithms for operations, which are optimized by using microcontroller-dependent instruction codes to boost the sensor node's capability and (5) miniaturized hardware system fabricated as a printed circuit board (PCB) for a high quality prototype and enclosed by waterproof plastic box for applications to real structures.

The proposed wireless sensor node is composed of four functional subsystems: (1) sensing interface, (2) computational core, (3) wireless transceiver and (4) power supply. The "sensing interface" includes an interface to which a piezoelectric sensor and a temperature sensor can be connected, and an impedance chip (AD5933) for exciting a piezoelectric sensor and measuring the impedance signals. Here, NTC (Negative Temperature Coefficient) disc thermistor is equipped for temperature sensing on the structure near a piezoelectric sensor. It is a low-cost and small-size resistance type device, and is suitable for temperature ranges from -20 °C to +120 °C with reference resistance of 10 k Ω at 25 °C. The "computational core" consists of a microcontroller and a serial flash memory for computational tasks and system operations with various embedded algorithms. Through embedding technologies in microcontroller, the wireless traffic can be reduced and the survival rate of transmitted data can be increased. In this sensor node, ATmega128L is adopted because it is one of high performance and low power 8-bit microcontrollers, and has 128 kilobytes of in-system self-programmable flash program memory (www.atmel.com). The "wireless transceiver" is an integral component of the wireless system, which is composed of a RF transceiver (CC2420), a balun transformer, and an antenna to communicate with a base station (K mote-B radio module) and/or other wireless sensor nodes and to broadcast the structural condition. CC2420 is a single chip 2.4 GHz IEEE 802.15.4 compliant RF transceiver designed for low-power and low-voltage wireless applications (www.ti.com). It provides a low-cost and highly integrated solution for robust wireless communication and extensive hardware support for



(a) wireless impedance sensor board (PCB)



(b) block diagram

Fig. 3 Proposed wireless impedance sensor node

packet handling, data buffering and burst transmission. These features reduce the load on the host controller and allow CC2420 to interface low-cost microcontrollers. The sensor node can be operated by one of three type “power supply” systems: 5 V AC-plug DC adapter, 3.6-7.2 V battery, or 5 V solar power system. The power can be monitored on the microcontroller using a general ADC, which transforms the analog signals acquired from batteries to the digital signals. For stable power supply to the sensor node during operations, LDO (Low-dropout regulator) is mounted for providing a fixed 3.3 V reference output to the sensor node. Solar power system for energy harvesting consists of single crystalline silicon solar cells ($120 \times 60 \text{ mm}^2$) to generate the maximum power for its size, two AA Ni-MH rechargeable batteries to stand high temperature and overcharging under sunlight and to last up to 1000 charge/discharge cycles, and a step-up DC/DC solar controller to protect the appliances and the batteries with over discharge prevention circuit. Fig. 3 shows the impedance sensor node developed in

Table 1 Features of the proposed wireless impedance sensor node

Output frequency range	1 ~ 100 kHz
Output frequency resolution	> 1 Hz
Impedance range	1 k Ω ~ 1 M Ω
Temperature range	-20 ~ 120 °C
Temperature resolution	> 0.03 °C
On-board processing	Yes (MCU : ATmega128L)
Operating frequency	2.4 GHz IEEE 802.15.4 / Zigbee RF transceiver
Outdoor transmission range	150 m (2dBi Dipole Antenna)
Power supply options	5V AC-plug DC adapter; Commercial batteries (3.6-7.2 V); Ni-MH rechargeable batteries with solar panels (5 V)
Feature	150 × 100 × 70 (mm); 310 (g)

this study and its block diagram, and the features are described in Table 1.

The developed impedance sensor node was tested on the several operational conditions to determine the actual in-service power consumption. A multimeter was placed in line on the node's positive voltage terminal. The current draw during each condition was recorded as: 1.3 mA in idle state, 25.8 mA during measurement, 15.2 mA during calculation, and 27.3 mA during transmission, which indicates that the maximum required power is approximately 90 mW with 3.3 V. It is slightly larger than the required power of 60 mW by Overly *et al.* (2008), which may be caused by additionally equipped NTC thermistor for temperature sensing, three LEDs for informing the node status by twinkling with different colors, and other operation subsystems. The required power may be reduced further with proper use of sleep modes in Overly *et al.* (2008).

3.2 Data control and on-board data analysis

TinyOS is the most typical open-source operating system designed for wireless embedded sensor networks. It features a component-based architecture which enables rapid innovation and implementation while minimizing code size as required by the severe memory constraints inherent in sensor networks. The proposed sensor node is based on TinyOS for system operation. On the other hand, the server is controlled by users through MATLAB[®] software, which is a high-level language and interactive environment to perform computationally intensive tasks faster than traditional programming languages such as C, C++, or FORTRAN, and includes a number of mathematical functions including Fourier analysis, filtering, signal processing and serial communications. Moreover, it provides GUI (graphical user interface) development environment, from which the user can easily change the control variables and monitor the wirelessly transmitted raw and/or processed data, temperature and node status such as battery condition. The serial communication is established between a server and a base station using two service daemons, which are cross-compiled using Cygwin. These daemons provide a Linux-like environment for Windows, and enable to communicate between MATLAB[®] (Windows) and base station/sensor node (TinyOS).

For continuous and autonomous SHM using wireless sensor nodes, it is strongly required to construct the embedded data analysis system. More power-efficient wireless SHMs could be achieved, if the measured impedance is analyzed on microcontroller of the sensor node and only the analyzed results

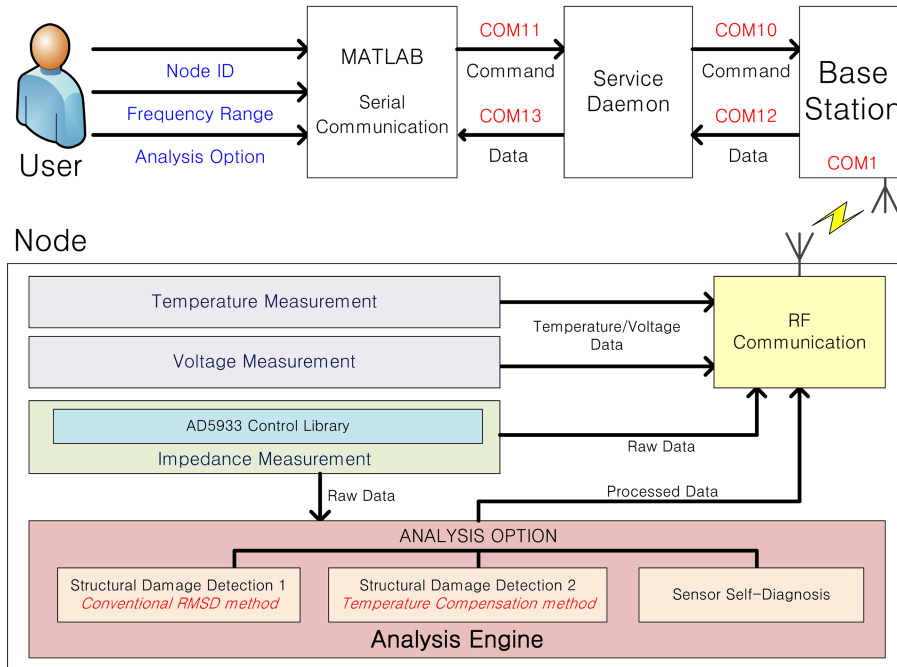


Fig. 4 Overall command/data flow of embedded software

could be wirelessly sent to a base station. Especially, this fact is crucial for self-powered wireless sensor nodes incorporating several kinds of energy harvesters. In the proposed sensor node, multifunctional algorithms are implemented for temperature/power measurement, impedance measurement and analysis engine for both structural damage detection and sensor self-diagnosis, as shown in Fig. 4. The impedance measurement block consists of the TWI library, AD5933 control library and the default sweep function (512 points) library. Using raw data from the impedance measurement block, the embedded analysis engine optionally performs the analysis for structural damage detection and sensor self-diagnosis. Two algorithms are embedded on the microcontroller for the structural status monitoring: the RMSD metric and the temperature compensated CC metric calculated by EFS method. Sensor self-diagnosis is simply carried out calculating the slope of the imaginary part of admittance. Here, the baseline impedance is stored at the serial flash memory. Depending on input arguments, the users can get raw or processed data from the designated sensors.

3.3 Self-powered wireless system incorporated with solar cells

Power scavenging enables “place-and-forget” wireless sensor node. Considering that the necessary cost and efforts for battery maintenance and replacement may over-shadow the merits of the wireless SHM system, the ability to scavenge energy from the environment is a quite important and it permits deploying self-powered sensor nodes onto inaccessible locations. Thus, many researchers have shown interest in power scavenging and the related technologies have steeply grown. Especially, the solar power is most often used, which is produced by collecting sunlight and converting it into electricity. This is done by using solar panels, which are large flat panels made up of many individual solar cells.

In this study, a solar power system for operating a wireless sensor node is designed with single



Fig. 5 Sensor node with a solar panel

crystalline silicon solar cells ($120 \times 60 \text{ mm}^2$), two AA Ni-MH rechargeable batteries ($1.2 \text{ V} \times 2\text{ea}$), and a step-up DC/DC solar controller, considering one-time measurement per day. A step-up DC/DC solar controller offers 4.8 V reference output from a lowered battery voltage of more than 2 V. This solar power system provides maximum 750 mW, which may be enough to operate the developed sensor node of 90 mW. If the larger power is needed for more frequent measurements per day, the recharging capacity of the solar power system may be increased by using higher-efficient and bigger-size solar panels and higher-voltage batteries. To validate the ability of the solar power system, a simple experiment has been carried out on an aluminum plate as shown in Fig. 5. A macro-fiber composite (MFC) patch of $47 \times 25 \times 0.267 \text{ mm}^3$ (2814P1 Type; Smart Material[®]) was surface-bonded to the aluminum specimen of $50 \times 1,000 \times 4 \text{ mm}^3$. The MFC is a relatively new type of PZT transducer that exhibit superior ruggedness and conformability compared to traditional piezoceramic wafers.

At the beginning, the batteries were fully recharged by an electric battery charger. Then, the experiment started at 00:00 am on 6 September, 2009. Raw impedance signals and the processed structural damage detection results were wirelessly transmitted to a base station at every 10:00 am for five days. The weather condition was changed in five days as follows: sunny ($19.6\text{-}31.1 \text{ }^\circ\text{C}$; cloud 0.8),

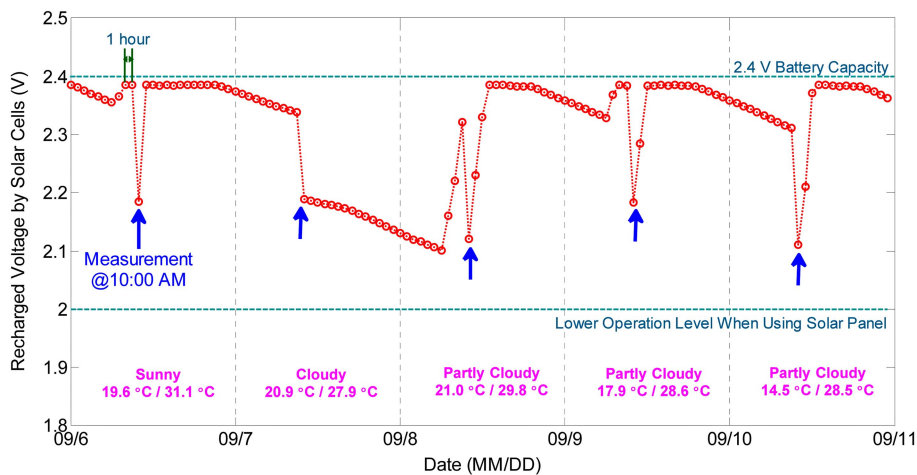


Fig. 6 Voltage monitoring of a wireless SHM system with solar cells

mostly cloudy (20.9-27.9 °C; cloud 7.6), partly cloudy (21.0-29.8 °C; cloud 5.3), partly cloudy (17.9-28.6 °C; cloud 4.3), and partly cloudy (14.5-28.5 °C; cloud 6.8). Fig. 6 shows the voltage level in two AA rechargeable batteries during five days, which was measured every one hour. Although the voltage steeply declined during the measurement of impedances and on-board calculation of damage index, it was almost fully recovered in one hour under sun light. It may indicate that it is able to operate the sensor node several times per day. The recharged voltage remained on stable condition under sun light, but it decreased at 0.005 V/hour at night. When cloudy, the solar cells could not be recharged due to the lack of sun light, but it shortly returned to stable condition as the sun rose. From the above results, it may be concluded that the solar power system is able to provide a solution for maintenance-free wireless sensor nodes in spite of sensitive reaction to the environment, which would be complemented by development of the more efficient energy scavenging technologies.

4. Performance validation of wireless impedance sensor node

To investigate the performance of the wireless impedance sensor node designed and fabricated in this study, a series of experiments have been performed for structural damage identification and sensor self-diagnosis. First, the performance for impedance measurement was evaluated on an aluminum plate. Impedances measured using the wireless sensor node were compared with the impedance measured using the conventional impedance analyzer, HP4294A. Second, damages detection was carried out on a steel truss member to validate the embedded software in the sensor node. Third, experiments for sensor self-diagnosis were carried out to detect PZT sensor's defects and bonding layer's defects. For all of the testing performed, the wireless sensor node was powered by one 3.6 V battery. Once the measurement and data analysis were carried out in the sensor node, they were wirelessly sent to a Kmote-B radio module with a CC2420 RF transceiver that was used as a serial port interface. MATLAB[®] was used to import both raw data and/or on-board processed CC indices from the RF communications and to plot all the results on the end-user server PC.

4.1 Evaluation of impedance measurements on an aluminum plate

It is crucially important to validate how exactly the impedance sensor node can measure the E/M impedances for SHM applications. Therefore, the measured impedance signatures have been examined on a simple plate made from a 6063 T5 aluminum alloy. A MFC patch of $47 \times 25 \times 0.267 \text{ mm}^3$ (2814P1 Type; Smart Material[®]) was surface-mounted using superglue (cyanoacrylate adhesive) on the specimen of $25 \times 275 \times 1 \text{ mm}^3$. The test setup is shown in Fig. 7.

The impedances were recorded in a frequency range of 40-80 kHz using both a conventional impedance analyzer (HP4294A) and the wireless impedance sensor node utilizing AD5933. Fig. 8 shows the real parts and the imaginary parts of impedances obtained from both equipments. In these figures, same peak frequencies can be observed at two signatures measured by HP4294A and AD5933, although the magnitudes of the peaks and the shapes of the troughs are quite different. The difference in two signatures may be caused by the A/D conversion and the inherent electrical impedances of the internal chips. The sensing resistor of AD5933 to estimate the impedance value in the sensor node also contributes to the differences in magnitude (Overly *et al.* 2008). However, it does not seem to cause significant problems for SHM, because the impedance-based SHM is based on the relative difference between two normalized signals in the healthy and the concurrent conditions and

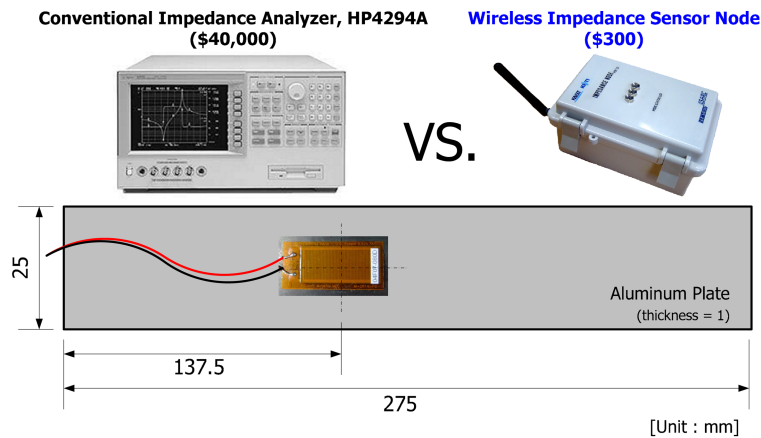


Fig. 7 Test specimen and experimental setup for measuring impedances

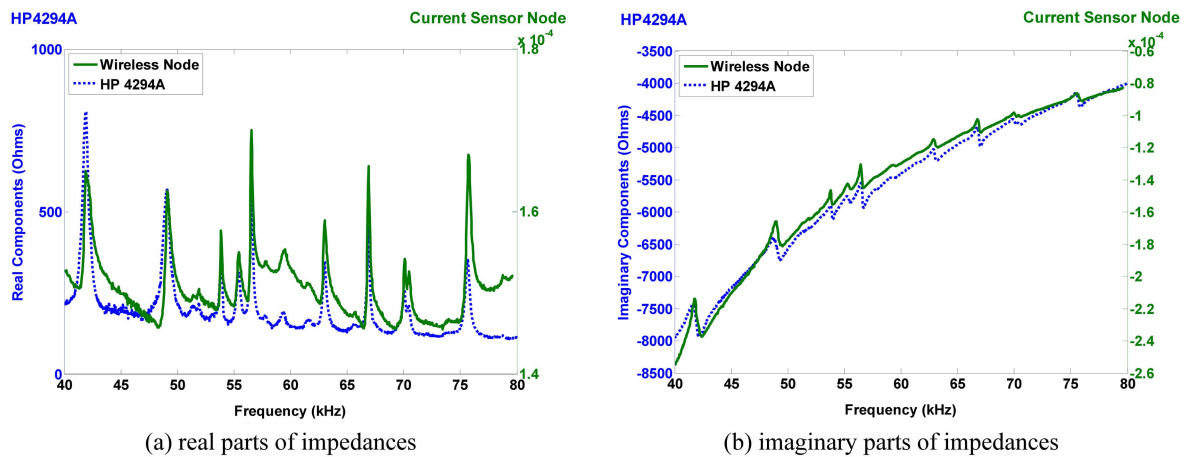


Fig. 8 Performance of the developed wireless impedance sensor node compared with HP4294A

the inherent differences in magnitude may be canceled out. Furthermore, the damage indices in Eqs. (2) and (3) are based on the sum of squares of the differences, so possible errors in the measurements around the troughs do not cause significant effect to the damage indices. The current wireless sensor node is very cost-effective for real SHM applications to large structures considering that its cost is approximately 300 USD, while the cost of HP4294A is about 40,000 USD.

4.2 Damage detection on a steel truss member

The second experiment was carried out to check the feasibility of damage detection on a steel truss member under temperature varying condition. A MFC patch of $47 \times 25 \times 0.267 \text{ mm}^3$ (2814P1 Type; Smart Material[®]) was mounted using superglue on the surface of the laboratory-scale model ($150 \times 150 \times 530 \text{ mm}^3$) of a vertical truss member of Seongsu Bridge, Korea, which caused the collapse the bridge in 1994. The specimen is composed of two segments with wide flange sections of different flange thicknesses of 6 and 3 mm welded together as in Fig. 9. An artificial crack was inflicted by

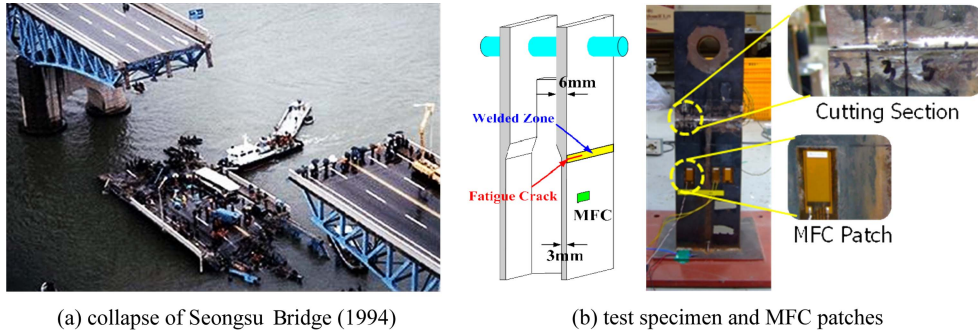


Fig. 9 Laboratory-scale model of a steel truss member of Seongsu Bridge

cutting the flanges sequentially (10, 20, 30 and 40 mm) using electric saw on the left side of the welded zone. The MFC patch was attached at a location 120 mm apart from the crack. Then the increase of the crack length is monitored using the wireless sensor node. The maximum temperature variation obtained from a NTC thermistor was 10 °C.

To test the ability of the embedded structural damage diagnosis algorithm in the microprocessor, the impedance measurements in the frequency range of 46.5-51.5 kHz were taken for an intact and each of four damage cases as shown in Fig. 10. It is clear from this figure that real parts of impedances show large variations of peaks in the whole frequency range as the level of the crack length is also increased, while imaginary parts do not change remarkably. It means that the damage mainly affects on the real part of the impedance rather than on the imaginary part (Bhalla *et al.* 2002). Then, both conventional and temperature-compensated CC values, defined in Eqs. (3) and (4), were calculated using real parts of impedances as shown in Fig. 11. It should be noted that temperature-compensated CC values were computed in the microprocessor of the sensor node. The conventional CC metric showed fairly large fluctuation due to the temperature variation even at the same damage condition and could not correctly distinguish Cases II and III, but the temperature-compensated CC damage metric clearly identified the all damage cases by showing significant distinctions for different damage severities.

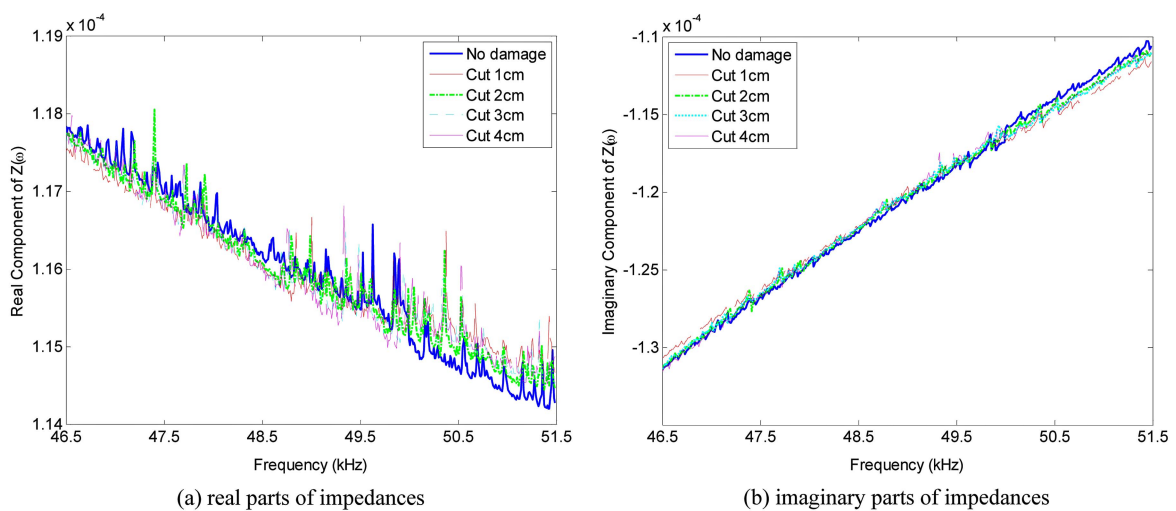


Fig. 10 Measured impedance signatures at baseline and damage cases

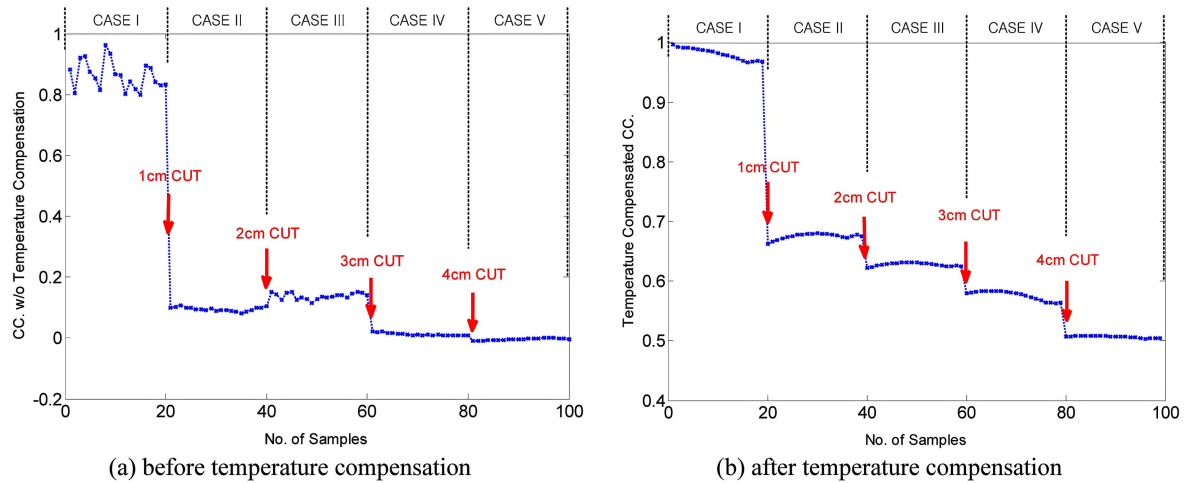


Fig. 11 Temperature-compensated crack damage detection on a steel truss member

4.3 Sensor self-diagnosis using embedded software

A piezoelectric sensor diagnostic procedure based on electrical admittance measurements was implemented in the developed sensor node. The basis of the sensor diagnostic procedure is to track changes in the capacitive value of piezoelectric materials manifested in the imaginary parts of the measured electrical admittances. The structural damage induces changes in the real parts of the admittance signatures, while the sensor failure results in changes to the imaginary parts of the admittance signatures distinctively causing a decrease (sensor breakage) and an increase (de-bonding between PZT transducers and the host) in the capacitive value (Park *et al.* 2006).

In order to determine the performance of the sensor node in sensor diagnosis, an experiment was carried out on an aluminum plate of $1000 \times 1100 \times 1 \text{ mm}^3$ as in Fig. 12. First, four PZTs (PIC151 Type; PI[®]) with different sizes (1/4-, 1/2-, 3/4- and full sized) were surface-attached using superglue on an aluminum plate to investigate the effects of sensor's fracture. The perfect size of the sensor is $10 \times$

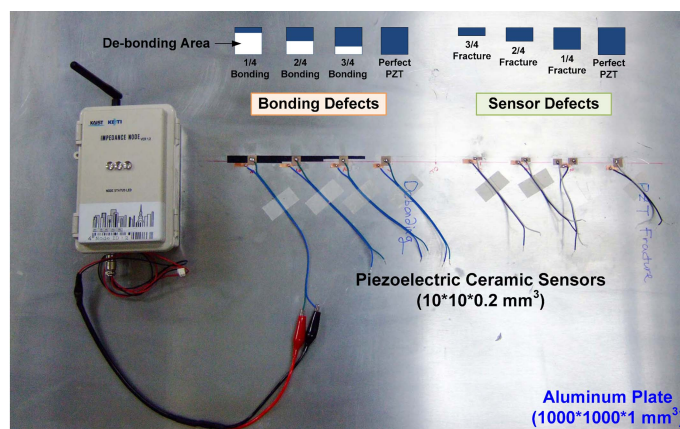


Fig. 12 Experimental setup for investigation of the piezoelectric sensor diagnosis

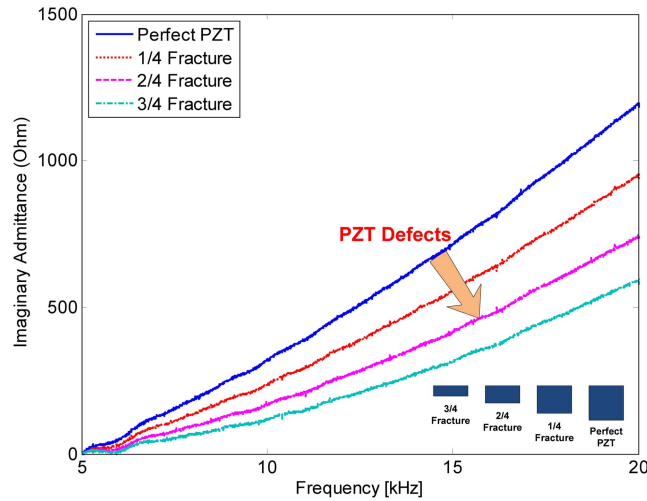


Fig. 13 Effects of PZT sensor’s fracture

$10 \times 0.2 \text{ mm}^3$. Second, other four PZTs (PIC151 Type; PI[®]) with different bonding area (1/4-, 1/2-, 3/4- and perfect bonding) were also attached on the surface of the same aluminum plate to see the effects of the bonding layer’s defects. Cellular tapes were used between the sensors and the plate to simulate different de-bonding areas. Admittances were measured in the frequency range of 5-20 kHz using the sensor node. All experiments were carried out under the same temperature environment (approximately 24 °C).

Fig. 13 shows that the slope of the imaginary parts of the measured admittances decreases, as the severity of the PZT fracture increases. The sensor breakage causes a reduction in the capacitance of the PZT, which is related to the sensor quality index, a , in Eq. (5). In contrast, the increase of the de-bonding area makes slope of the imaginary parts of the admittances to increase, as shown in Fig. 14. The bonding layer’s defects are related to the bonding degradation index (b) and shear-lag index (ξ) between the bonding layer and the host structure. The present results are well-consistent with the

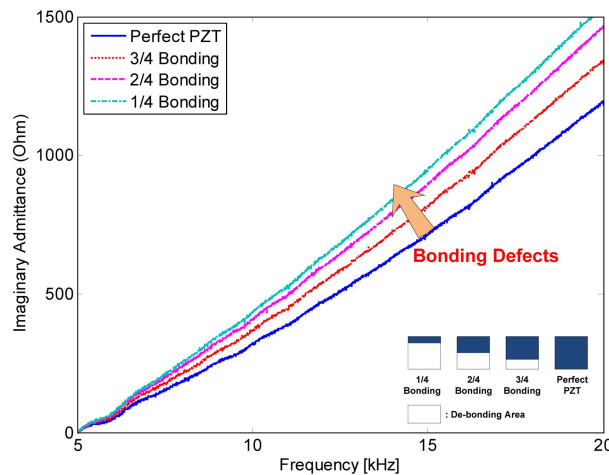


Fig. 14 Effects of de-bonding of PZT sensor

previous experimental and numerical investigations of other researchers (Park *et al.* 2006, Overly *et al.* 2008, Park *et al.* 2009b).

5. Field applications

For the case of steel structures, most common damage types would be: 1) loose bolts at bolt-jointed members, 2) fatigue cracks at the critical members, and 3) welding defects. In this study, a series of experimental works were performed using the developed impedance sensor node to detect loosened bolts and artificial crack damages inflicted on real building and bridge structures. For all of the testing performed, the wireless sensor node was powered using one 3.6 V battery. The temperature on the structure near a PZT sensor and the voltage of the battery were monitored before impedance measurement. Temperature-compensated CC indices calculated in the microprocessor using measured impedance signals were wirelessly sent to a Knote-B RF module. MATLAB[®] imported on-board processed CC values from the RF communications and plotted the results on the end-user server PC.

5.1 Loose bolt detection at the base of a steel column

The first test was carried out to monitor loosened bolts at the base of an inclined steel column (diameter of 180 mm) for a building roof as shown in Fig. 15. The base plate ($600 \times 300 \times 10 \text{ mm}^3$) is fixed to a concrete base by four bolts with a diameter of 19 mm. One sensor node was installed beside the concrete base, and connected to a PZT of $30 \times 30 \times 0.5 \text{ mm}^3$ (PIC151 Type; PI[®]) and a NTC thermistor bonded near Bolt #1. The monitoring of the bolted base plate started with the as-built condition without measuring the torques on the bolts. The test was carried out for 2 days. The maximum temperature variation obtained from a NTC thermistor was approximately 15 °C.

Assuming that all the bolts were on healthy condition, E/M impedances were measured at a frequency range of 45-50 kHz and their averaged data was stored as a baseline data. This frequency range was chosen as it contains a significant dynamic interaction between the PZT and the structure with multiple resonant peaks. Then, four damage scenarios were imposed by increasing the number of bolts loosened by one full rotation in a sequence, of which the locations are described in Fig. 15. Twenty measurements were carried out for each damage case. Each measurement took about 1.5 minutes, and the interval of measurements was 25 minutes. Fig. 16 shows one set of impedance records for 5 damage cases. Then, temperature-compensated CC indices of Eq. (4) were calculated in the microcontroller unit of the sensor node and were wirelessly transmitted to the base station. Fig. 17

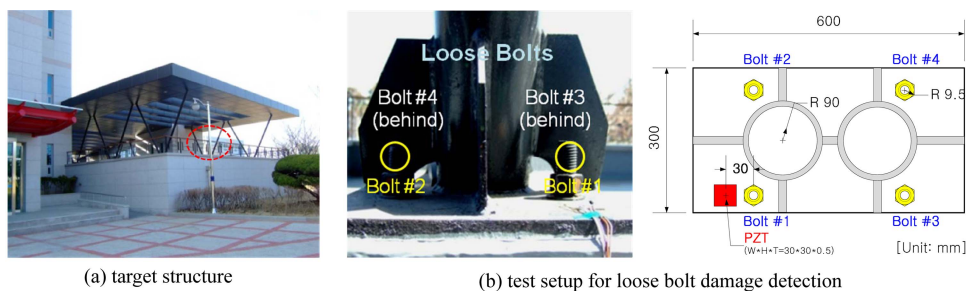


Fig. 15 Loosened bolt detection at the base of a steel column

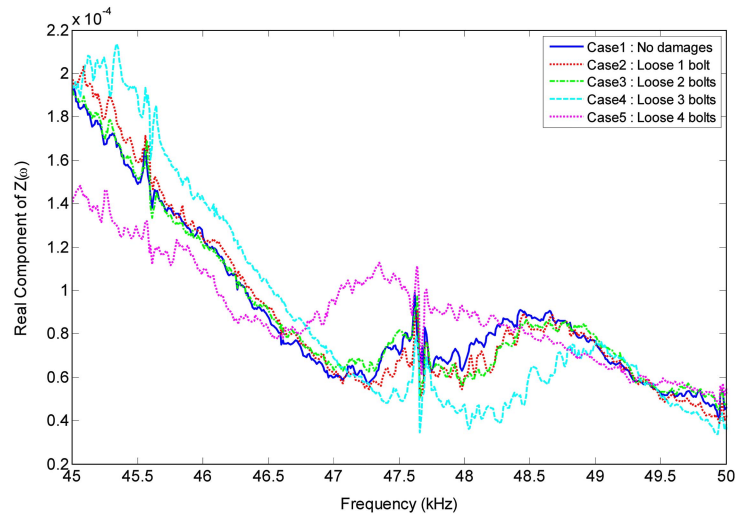


Fig. 16 Real parts of impedances between baseline (no damages) and loosened bolt damage cases

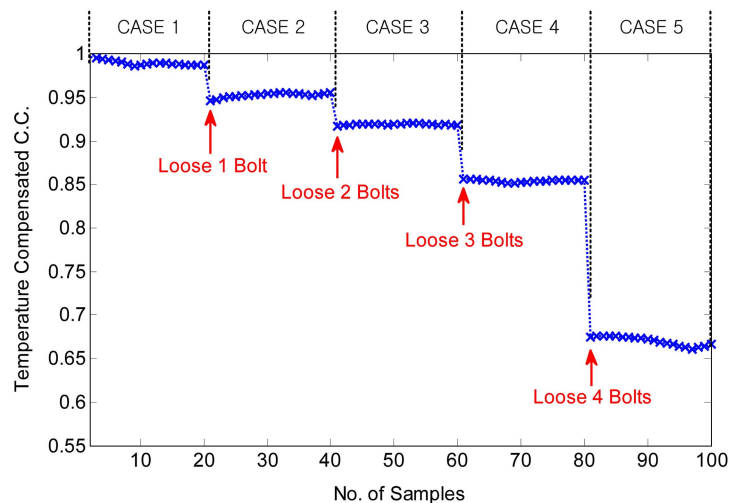


Fig. 17 Temperature-compensated CC results for loosened bolt detection on a building structure

shows that CC values decrease significantly and consistently, as the number of loosened bolts increases. During the tests for 100 measurements in 2 days, the voltage drop in the battery was only 0.004 V from 3.483 V to 3.479 V.

5.2 Multiple damage detection on a steel girder of bridge structure

As another application for detecting damages including loosened bolts and notches, a field test has been performed on the Ramp-G bridge in Incheon, Korea. The bridge is a conventional steel box girder bridge with a reinforced concrete deck as shown in Fig. 18. It has 2 continuous spans with a total length of 90 m. The bridge has been decommissioned, so small damages could be inflicted with an authorization of the Korea Expressway Corporation. One sensor node was installed near the bolted

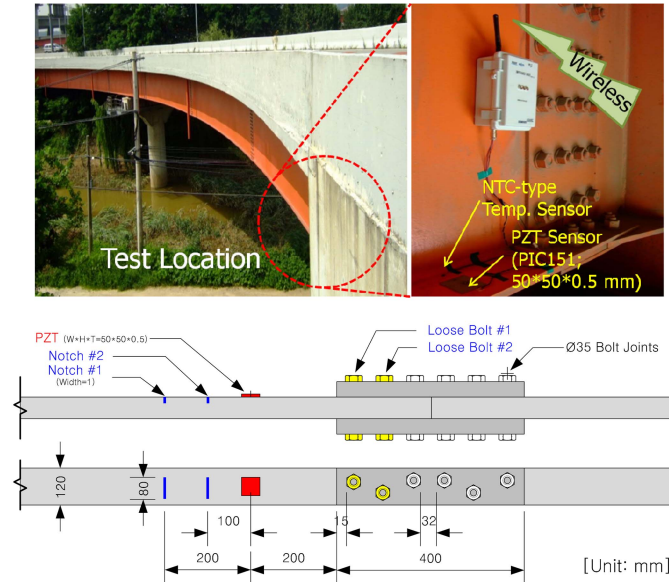


Fig. 18 Experimental setup for impedance-based SHM on Ramp-G bridge

Table 2 Damage scenarios for detecting multiple damages on a bridge girder

Case	Damage description	Case	Damage description
1	No damages	5	Additionally loosen Bolt #1 (2 Turns)
2	Loosen Bolt #1 (2 Turns)	6	Additionally loosen Bolt #2 (2 Turns)
3	Hand-retighten Bolt #1	7	Additionally apply Notch #2
4	Apply Notch #1	-	-

joint of the outer girder and connected to a PZT patch of $50 \times 50 \times 0.5 \text{ mm}^3$ (PIC151 Type; PI[®]) and a NTC thermistor surface-mounted at a distance of 200 mm from the bolted joint using epoxy glue. The maximum temperature variation measured from a NTC thermistor was 15°C during the test of 2 days, and the voltage drop in the battery was 0.004 V from 3.476 V to 3.472 V.

The E/M impedances were measured at a frequency range of 45-50 kHz for the baseline. The frequency range was chosen as it contains a significant dynamic interaction between the PZT and the structure. Here, it was assumed that there were not damages in the initial condition (Case I). A series of damages were imposed as in Table 2, and tests were carried out for each case. The first damage was simulated by loosening Bolt #1 by two rotations, and then Bolt #1 was hand-tightened using a wrench. Cracks and multiple damages were induced in a sequence. Measurements were carried out 10 times for each damage case. Example cases of the measured impedance signals at different damage conditions were compared with the baseline data in Fig. 19, from which significant variations are observed for different damage cases. Fig. 20 shows temperature-compensated CC values, which were computed in the on-board microcontroller and wirelessly transmitted to a base station. It can be observed that the CC value decreases when Bolt #1 gets loosened, and it recovers almost fully as the bolt is hand-tightened. Then, the CC value decreases consistently as the damage severity increases by additional loosened bolts and artificial notches. The CC metrics for Cases 5 and 6 are found to be similar, which may be because Bolt #2, which got loosened in Case 6, is located fairly far from the sensor.

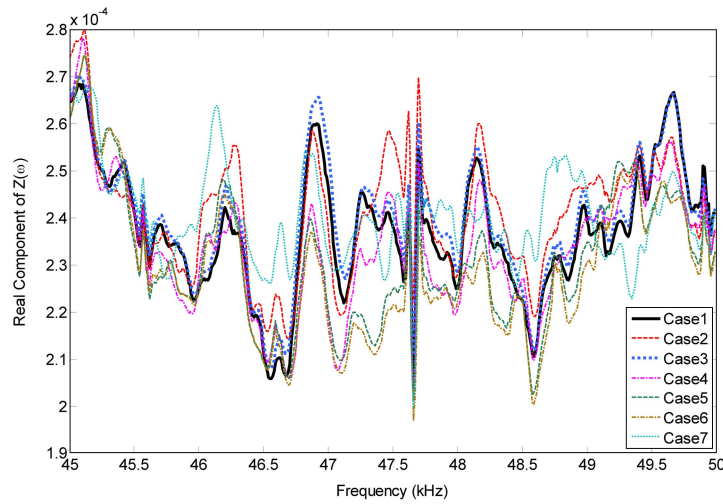


Fig. 19 Measured impedance signatures at various damage cases

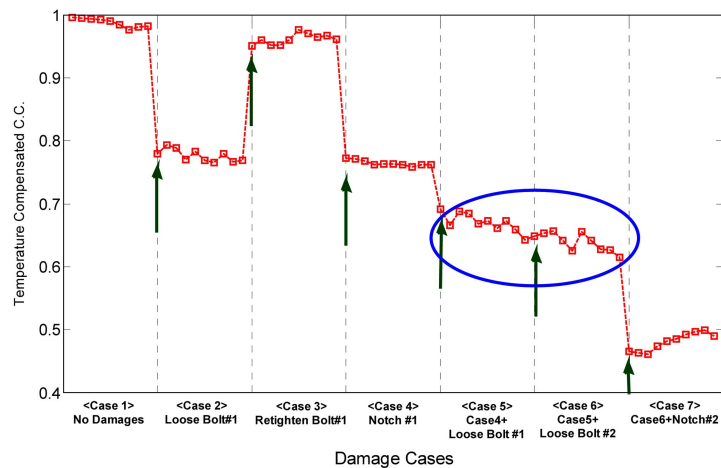


Fig. 20 Temperature-compensated CC indices for multiple damage detection on a bridge

6. Conclusions

This paper presented the development of a low cost, low power but multifunctional wireless impedance sensor node for online structural health monitoring, which is incorporating an impedance chip (AD5933) for exciting a PZT sensor and measuring the impedance signals, a microcontroller (ATmega128L) for controlling and on-board signal processing, and a RF module (CC2420) for wirelessly transmitting the data to end-user PC. This sensor node can be operated using the power harvested from solar energy. For on-board signal processing, algorithms for the temperature-compensated damage detection and sensor-self diagnosis are embedded in the microcontroller based on an open-source operating system, TinyOS. Monitoring capability for temperature and power consumption is added. MATLAB[®]-GUI is utilized to import the raw and/or processed data from the RF communications, and plot the data on the end-user server PC. The applicability of the proposed wireless sensor node was

successfully demonstrated through a series of experimental studies for detecting loosened bolts and crack damages on laboratory-scale steel structural members and members of real building/bridge structures. The results indicate that the current wireless impedance sensor node can effectively detect structural damages and sensor damages. It is expected that the wireless impedance sensor node plays an important role in the development of cost-effective online SHM system for critical structural members.

Acknowledgements

This work was jointly supported by the Smart Infra-Structure Technology Center (SISTeC) at KAIST sponsored by the National Research Foundation (Grant No. R11-2002-101-03001-0), the 2006 C&T Innovation Program (Grant No. 06coretech-B05), and a Cutting-edge Urban Development - Korean Land Spatialization Research Project (Grant No. 06KLSGC01) sponsored by Ministry of Land, Transport and Maritime Affairs of Korean Government. Their financial supports are greatly appreciated. Finally, the authors would like to thank Dr. Chang-Geun Lee of Korea Expressway Corporation (KEC) for giving a chance to perform field tests at Ramp-G bridge.

References

- Bhalla, S., Naidu, A.S.K. and Soh, C.K. (2002), "Influence of structure-actuator interactions and temperature on piezoelectric mechatronic signatures for NDE", *Proceedings of the ISSS-SPIE International Conferences on Smart Materials Structures and Systems*, Bangalore, December.
- Giurgiutiu, V., Reynolds, A. and Rogers, C.A. (1999), "Experimental investigation of E/M impedance health monitoring of spot-welded structure joints", *J. Intel. Mat. Syst. Str.*, **10**, 802-812.
- Giurgiutiu, V., Zagari, A.N. and Bao, J.J. (2002), "Piezoelectric wafer embedded active sensors for aging aircraft structural health monitoring", *J. Struct. Health Monit.*, **1**, 41-61.
- Giurgiutiu, V. (2008), *Structural health monitoring with piezoelectric wafer active sensors*, Amsterdam: Elsevier/Academic Press.
- Grisso, B.L. and Inman, D.J. (2005), "Developing an autonomous on-orbit impedance-based SHM system for thermal protection systems", *Proceedings of the 5th Int'l Workshop on Structural Health Monitoring*, Stanford, CA, September.
- Koo, K.Y., Park, S., Lee, J.J. and Yun, C.B. (2009), "Automated impedance-based structural health monitoring incorporating effective frequency shift for compensating temperature effects", *J. Intel. Mat. Syst. Str.*, **20**, 367-377.
- Liang, C., Sun, F.P. and Rogers, C.A. (1996), "Electro-mechanical impedance modeling of active material systems", *Smart Mater. Struct.*, **5**, 171-186.
- Lynch, J.P., Sundararajan, A., Law, K.H., Sohn, H. and Farrar, C.R. (2004), "Design of a wireless active sensing unit for structural health monitoring", *Proceedings of the SPIE Annual Int'l Symposium on Smart Structures and Materials*, San Diego, CA, March.
- Mascarenas, D.L., Todd, M.D., Park, G. and Farrar, C.R. (2007), "Development of an impedance-based wireless sensor node for structural health monitoring", *Smart Mater. Struct.*, **16**, 2137-2145.
- Mascarenas, D.L., Park, G., Farinholt, K., Todd, M.D. and Farrar, C.R. (2009), "A low-power wireless sensing device for remote inspection of bolted joints", *Proceedings of the Institution of Mechanical Engineers, Part G: Journal of Aerospace Engineering*, **223**(5), 565-575.
- Overly, T.G., Park, G., Farrar, C.R. and Allemang, R.J. (2007), "Compact hardware development for structural health monitoring and sensor diagnostics using admittance measurements", *Proceedings of the IMAC-XXV: A Conference & Exposition on Structural Dynamics*, Orlando, FL, February.

- Overly, T.G., Park, G., Farinholt, K.M. and Farrar, C.R. (2008), "Development of an extremely compact impedance-based wireless sensing device", *Smart Mater. Struct.*, **17**(6).
- Park, G., Kabeya, K., Cudney, H.H. and Inman, D.J. (1999), "Impedance-based structural health monitoring for temperature varying applications", *JSME Int. J. A-Solid M.*, **42**, 249-258.
- Park, G., Sohn, H., Farrar, C.R. and Inman, D.J. (2003), "Overview of piezoelectric impedance-based health monitoring and path forward", *Shock Vib. Digest*, **35**, 451-463.
- Park, G., Farrar, C.R., Rutherford, A.C. and Robertson, A.N. (2006), "Piezoelectric active sensor self-diagnostics using electrical admittance measurements", *J. Vib. Acoust.*, **128**, 469-476.
- Park, S., Yun, C.B., Roh, Y. and Lee, J.J. (2005), "Health monitoring of steel structures using impedance of thickness modes at PZT patches", *Smart Struct. Syst.*, **1**, 339-353.
- Park, S., Shin, H.H. and Yun, C.B. (2009a), "Wireless impedance sensor nodes for functions of structural damage identification and sensor self-diagnosis", *Smart Mater. Struct.*, **18**, 1-11.
- Park, S., Park, G., Yun, C.B. and Farrar, C.R. (2009b), "Sensor self-diagnosis using a modified impedance model for active sensing-based structural health monitoring", *J. Struct. Health Monit.*, **8**(1), 71-82.
- Peairs, D.M., Tarazaga, P.A. and Inman, D.J. (2006), "A study of the correlation between PZT and MFC resonance peaks and damage detection frequency intervals using the impedance method", *Proceedings of the International Conference on Noise and Vibration Engineering*, Leuven, Belgium, September.
- Saint-Pierre, N., Jayet, Y., Perrissin-Fabert, I. and Baboux, J.C. (1996), "The influence of bonding defects on the electric impedance of piezoelectric embedded element", *J. Phys. D. Appl. Phys.*, **29**, 2976-2982.
- Taylor, S.G., Farinholt, K.M., Park, G. and Farrar, C.R. (2009a), "Wireless impedance device for electromechanical impedance sensing and low-frequency vibration data acquisition", *Proceedings of the SPIE Annual International Symposium on Sensors and Smart Structures Technologies for Civil, Mechanical, and Aerospace Systems*, San Diego, CA, March.
- Taylor, S.G., Farinholt, K.M., Flynn, E.B., Figueiredo, E., Mascarenas, D.L., Moro, E.A., Park, G., Todd, M.D. and Farrar, C.R. (2009b), "A mobile-agent-based wireless sensing network for structural monitoring applications", *Meas. Sci. Technol.*, **20**(4).